

# FFT-based Methods for Nonlinear Image Restoration in Confocal Microscopy

J.B.T.M. Roerdink

*Department of Computing Science  
University of Groningen  
P.O. Box 800, 9700 AV Groningen  
The Netherlands*

Recently we developed a new method for attenuation correction in three-dimensional imaging by a confocal scanning laser microscope (CSLM) in the (epi)fluorescence mode. The fundamental element in our approach consisted in multiplying the measured fluorescent intensity by a correction factor involving a convolution integral of this intensity, which can be computed efficiently by the Fast Fourier Transform (FFT). The resulting algorithm is one or two orders of magnitude faster than an existing iterative method, but was found to have a somewhat smaller accuracy. In this paper we improve on this latter point by reformulating the problem as a statistical estimation problem. In particular we derive first order moment and cumulant estimators leading to a nonlinear integral equation for the unknown fluorescent density, which is solved by an iterative method where in each step a discrete convolution is performed using the FFT. We find that only a few iterations are needed. It is shown that the estimators proposed here are more accurate than the existing iterative method, while retaining the advantage in computational efficiency of the FFT-based approach.

*AMS 1991 Mathematics Subject Classification: 68U10, 78A99.*

*Keywords:* Fluorescence confocal microscopy, attenuation correction, convolution method, Fast Fourier Transform, moment estimator, cumulant estimator, 3D image restoration, iterative methods.

*Note:* Postscript version obtainable at <http://www.cs.rug.nl/~roe/>. Final version appeared in: *J. Math. Imaging and Vision* 4 (2), 1994, pp. 199-207.

## 1. Introduction

A major problem in three-dimensional (3D) imaging by a confocal scanning laser microscope (CSLM) in the (epi)fluorescence mode is the darkening of the deeper layers in the object due to scattering and absorption of excitation and fluorescence light [1,7]. A way has been

devised to correct for this effect by a layer stripping method, where one iteratively corrects the first, second etc. layer, see Visser et al. [6]. In a previous paper [5], hereafter referred to as Part I, we developed a new restoration method to correct for these effects. Assuming that the attenuation is weak, we constructed by analytic methods a correction factor to the standard restoration taking the form of a 3D convolution of the measured signal, which can be efficiently computed by the use of the Fast Fourier Transform (FFT). We therefore refer to this method as the ‘FFT-method’. In this way, the complexity of computation is reduced to  $O(N_z \log N_z)$ , where  $N_z$  is the number of vertical layers to be restored. The accuracy of the results depends on the depth of the layer considered: deeper layers are less accurately reconstructed than higher layers.

We also compared the computational efficiency of our algorithm with the iterative layer stripping method of [6], henceforth referred to as the ‘layer method’. In its original form this method has computational complexity  $O(N_z^4)$  which is unacceptably slow, taking many hours on a RISC workstation for a  $256 \times 256 \times 16$  image [6]. The layer method ‘with condensation’ developed in [6] in order to reduce the computation time, still has complexity  $O(N_z^2)$ . Thus, when the number of vertical layers gets larger the difference in computational efficiency with the FFT-method becomes increasingly pronounced. For spatially varying image densities the restoration quality using our method was found to be a little poorer than in the layer method.

In this paper we improve the accuracy of the FFT-method by reformulating the problem as a statistical estimation problem. In particular we derive first order moment and cumulant estimators leading to a nonlinear integral equation for the unknown fluorescent density, which is solved by an iterative method. It is shown that the new estimators, the moment estimator in particular, are more accurate than the layer method. Since only two or three iterations are needed and each iteration step involves a discrete 3D convolution computable by the FFT, the advantage in computational efficiency over the layer method is retained.

The organization of this paper is as follows. In Section 2 we review the mathematical model of the imaging process of the CSLM leading to a nonlinear integral transform of the object function, and review the solution method of Part I. In Section 3 we then reformulate the CSLM transform as a statistical averaging problem and derive the corresponding first order moment and cumulant estimators. The resulting nonlinear integral equations for the object density can be solved by an iterative method, which is described in Section 4. We apply our method in Section 5 to the test images used in Part I, and present results on the restoration accuracy. Section 6 contains a summary and conclusions.

## 2. The CSLM transform

The imaging process of a CSLM operating in the fluorescence mode was described in detail in Part I. A laserbeam is focussed upon a pinhole, expanded again and, through a system of lenses, focussed upon a point  $\mathbf{r} = (x, y, z)$  in the object. Here the  $z$ -direction is chosen along the optical axis. The rays converging to the object point are contained in a circular cone (‘light cone’) with angle  $\omega$ , called the ‘semi-aperture angle’, see Figure 1. The radiation absorbed at the point in focus is uniformly reemitted as fluorescent radiation and the part which travels back the same route as the incoming radiation is detected. The object is discretized into a number  $N_z$  of layers along the optical axis, a distance  $\delta_z$  apart. The total depth of the sample is denoted by  $d_z$ . Also, each layer is discretized into a rectangular grid of  $N_x$  by  $N_y$  points, with spacings  $\delta_x$  and  $\delta_y$  in the  $x$ - and  $y$ -direction, respectively. By moving the scan table of the CSLM each objectpoint of the 3D grid so formed is brought into focus and the corresponding fluorescent intensity (energy per unit of time) measured.

As a result, the measured fluorescent intensity  $f(\mathbf{r})$  can be expressed as the following nonlinear integral transform ('CSLM-transform') of the unknown fluorescent density  $\rho(\mathbf{r})$ ,

$$f(\mathbf{r}) = \rho(\mathbf{r}) \times \gamma_f(\mathbf{r})\gamma_b(\mathbf{r}), \quad (2.1)$$

where

$$\gamma_f(\mathbf{r}) := C_f \int_0^\omega d\theta \int_0^{2\pi} d\phi \sin\theta \cos\theta \exp\left[-\epsilon \int_0^z \frac{dz'}{\cos\theta} \rho(\hat{\mathbf{r}})\right] \quad (2.2)$$

is the forward attenuation factor, and

$$\gamma_b(\mathbf{r}) := C_b \int_0^\omega d\theta \int_0^{2\pi} d\phi \sin\theta \exp\left[-\epsilon \int_0^z \frac{dz'}{\cos\theta} \rho(\hat{\mathbf{r}})\right] \quad (2.3)$$

is the backward attenuation factor (both factors equal unity if there is no attenuation). In these equations  $\epsilon$  is a proportionality constant and

$$C_f := \frac{1}{\pi \sin^2\omega}, \quad C_b := \frac{1}{2\pi(1 - \cos\omega)}, \quad (2.4)$$

are the normalization constants referring to the forward and backward attenuation factors, respectively. Here  $\hat{\mathbf{r}}$  is the vector

$$\hat{\mathbf{r}}(\mathbf{r}; \theta, \phi, z') = (x + (z - z') \tan\theta \cos\phi, y + (z - z') \tan\theta \sin\phi, z'). \quad (2.5)$$

As  $z'$  runs from 0 to  $z$  this vector describes a light ray travelling to the point  $\mathbf{r} = (x, y, z)$  and making polar angles  $\theta$  and  $\phi$  with respect to the optical axis, cf. Figure 1.

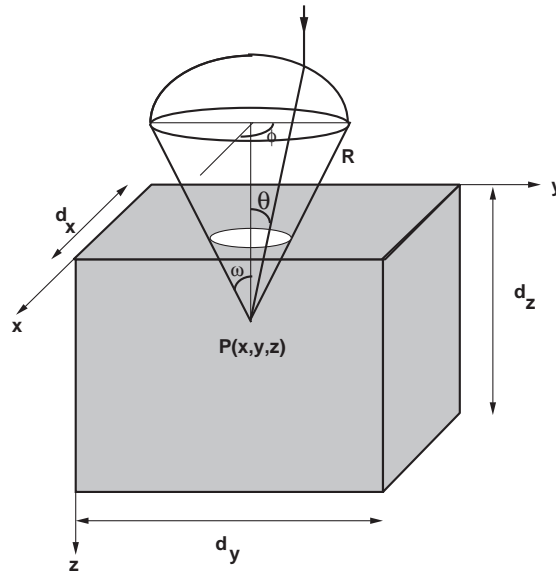


**Figure 1.** Geometry of light cone with apex at a point  $P(x, y, z)$  in the object.  $R$ : radius of spherical bundle;  $\omega$ : semi-aperture angle;  $(\theta, \phi)$ : polar angles of light ray;  $d_z$ : depth of the sample. The optical axis coincides with the  $z$ -axis.

A measure for the degree of attenuation of the signal when traversing the complete sample is provided by the dimensionless parameter  $\epsilon d_z$ , where  $d_z$  is the depth of the sample. Here we have restricted ourselves to the case that the attenuation is proportional to the fluorescent density. For a more general case see Part I.

### Inversion of the CSLM transform

By performing a perturbation expansion of the density  $\rho$  in the parameter  $\epsilon$  and collecting terms to first order in  $\epsilon$ , we derived in Part I the following approximation  $\tilde{\rho}(\mathbf{r})$  for the density,

$$\tilde{\rho}(\mathbf{r}) = f(\mathbf{r}) \{1 + \epsilon c(\mathbf{r})\}, \quad (2.6)$$

where  $c(\mathbf{r})$  is the convolution integral

$$c(\mathbf{r}) = \int_{-\infty}^{\infty} \int_{-\infty}^{\infty} \int_{-\infty}^{\infty} d\mathbf{r}' \kappa(\mathbf{r}') f(\mathbf{r} - \mathbf{r}'), \quad (2.7)$$

with  $\kappa(\mathbf{r})$  the space-invariant kernel given by

$$\kappa(x, y, z) = \begin{cases} C_f \frac{z}{(x^2 + y^2 + z^2)^{3/2}} + C_b \frac{1}{x^2 + y^2 + z^2}, & 0 \leq z \leq d_z, \quad x^2 + y^2 \leq (z \tan \omega)^2 \\ 0 & \text{elsewhere} \end{cases} \quad (2.8)$$

where it should be kept in mind that the densities  $f$  and  $\rho$  are only nonzero for  $0 \leq z \leq d_z$ . This means that to compute the value of  $c(x, y, z)$  only the part of the kernel between 0 and  $z$  has to be taken into account, see Figure 1.

### Numerical computation

For numerical computation, the integral (2.7) is discretized on a grid of  $N_x \times N_y \times N_z$  voxels, each voxel being a box of dimensions  $\delta_x, \delta_y, \delta_z$  in the  $x$ -,  $y$ - and  $z$ -directions. Then the approximation (2.6) is replaced by

$$R_{ijk} = F_{ijk}(1 + \epsilon C_{ijk}), \quad (2.9)$$

where

$$C_{ijk} = \sum_{i'=-\frac{M_x}{2}+1}^{\frac{M_x}{2}} \sum_{j'=-\frac{M_y}{2}+1}^{\frac{M_y}{2}} \sum_{k'=1}^{M_z} K_{i'j'k'} F_{i-i', j-j', k-k'}, \quad (2.10)$$

with

$$R_{ijk} := \tilde{\rho}(i\delta_x, j\delta_y, k\delta_z)$$

$$C_{ijk} := c(i\delta_x, j\delta_y, k\delta_z)$$

$$F_{ijk} := f(i\delta_x, j\delta_y, k\delta_z)$$

for  $(i, j, k)$  in the index set  $\mathbb{I} := \{(i, j, k) : i = 1, \dots, N_x; j = 1, \dots, N_y; k = 1, \dots, N_z\}$ , and it is tacitly understood that array elements are defined to be zero when the indices are not in the index set  $\mathbb{I}$  (so the third summation in Eq. (2.10) actually runs from 1 to  $k-1$ ). Here  $K$  is the discrete counterpart of the convolution kernel (2.8),

$$\begin{aligned} K_{ijk} &:= \int_{(i-\frac{1}{2})\delta_x}^{(i+\frac{1}{2})\delta_x} dx \int_{(j-\frac{1}{2})\delta_y}^{(j+\frac{1}{2})\delta_y} dy \int_{(k-\frac{1}{2})\delta_z}^{(k+\frac{1}{2})\delta_z} dz \kappa(x, y, z) \\ &\approx \delta_x \delta_y \delta_z \kappa(i\delta_x, j\delta_y, k\delta_z), \end{aligned} \quad (2.11)$$

and  $M_x = 2d_z \tan(\omega)/\delta_x$ ,  $M_y = 2d_z \tan(\omega)/\delta_y$  and  $M_z = d_z/\delta_z = N_z$  denote the support of the kernel in the three space directions, where in all cases rounding off to integer values is understood. The different treatment of the  $x, y$ -summations versus the  $z$ -summation stems from the fact that the kernel is symmetric in the  $x, y$ -directions, while it extends only over non-negative values in the  $z$ -direction. The discrete convolution (2.10) can be computed efficiently by FFT methods [5], see also [4].

### 3. Statistical estimators

It is useful to provide a probabilistic formulation of the CSLM-transform introduced above. To this end we notice that, by introducing the following ‘probability densities’ in  $\theta, \phi$ -space  $\{(\theta, \phi) : 0 \leq \theta \leq \omega, 0 \leq \phi < 2\pi\}$ ,

$$p_f(\theta, \phi) = C_f \sin \theta \cos \theta, \quad p_b(\theta, \phi) = C_b \sin \theta, \quad (3.1)$$

we can rewrite the basic transform (2.1) as

$$f(\mathbf{r}) = \rho(\mathbf{r}) \mathbb{E}_f \left( \exp \left[ -\epsilon \int_0^z \frac{dz'}{\cos \theta} \rho(\hat{\mathbf{r}}) \right] \right) \times \mathbb{E}_b \left( \exp \left[ -\epsilon \int_0^z \frac{dz'}{\cos \theta} \rho(\hat{\mathbf{r}}) \right] \right), \quad (3.2)$$

where  $\mathbb{E}_i$  denotes the mathematical expectation (statistical average) with respect to the density  $p_i, i = f, b$ .

Now we can apply moment and cumulant expansions of characteristic functions [2]. Performing the *first order moment expansion* for the random variable  $X(\theta, \phi)$ ,

$$\mathbb{E}_i (\exp[-\epsilon X(\theta, \phi)]) = 1 - \epsilon \mathbb{E}_i(X(\theta, \phi)) + \dots, \quad (3.3)$$

both for the forward and backward averages, we get

$$f(\mathbf{r}) \simeq \rho(\mathbf{r}) \left\{ 1 - \epsilon \int_0^{2\pi} d\phi \int_0^\omega d\theta C_f \sin \theta \int_0^z dz' \rho(\hat{\mathbf{r}}(\mathbf{r}; \theta, \phi, z')) \right\} \\ \times \left\{ 1 - \epsilon \int_0^{2\pi} d\phi \int_0^\omega d\theta C_b \tan \theta \int_0^z dz' \rho(\hat{\mathbf{r}}(\mathbf{r}; \theta, \phi, z')) \right\}. \quad (3.4)$$

Neglecting terms of order  $\epsilon^2$  and rewriting the sum of the two first order terms in convolution form as in Part I, Section 3, we obtain an equation for the ‘moment approximation’  $\rho^{(m)}(\mathbf{r})$  of Eq. (2.6),

$$f(\mathbf{r}) = \rho^{(m)}(\mathbf{r}) \left\{ 1 - \epsilon (\kappa * \rho^{(m)})(\mathbf{r}) \right\}, \quad (3.5)$$

where  $\kappa * \rho$  denotes the convolution of the functions  $\kappa$  and  $\rho$ , and the kernel  $\kappa$  is identical to that in Eq. (2.8).

Next we look also at the *first order cumulant expansion*,

$$\mathbb{E}_i (\exp[-\epsilon X(\theta, \phi)]) = \exp[-\epsilon \mathbb{E}_i(X(\theta, \phi)) + \dots], \quad (3.6)$$

for both averages. Then we find the ‘cumulant approximation’  $\rho^{(c)}(\mathbf{r})$  for the density, satisfying the equation

$$f(\mathbf{r}) = \rho^{(c)}(\mathbf{r}) \exp \left[ -\epsilon (\kappa * \rho^{(c)})(\mathbf{r}) \right], \quad (3.7)$$

where again the same kernel  $\kappa$  as above turns up. To solve Eq. (3.5) and Eq. (3.7) numerically, we rewrite them in the form

$$\rho^{(c)}(\mathbf{r}) = f(\mathbf{r}) \exp \left[ \epsilon (\kappa * \rho^{(c)})(\mathbf{r}) \right], \quad (3.8)$$

for the cumulant estimator, and

$$\rho^{(m)}(\mathbf{r}) = f(\mathbf{r}) \left[ 1 - \epsilon (\kappa * \rho^{(m)})(\mathbf{r}) \right]^{-1}, \quad (3.9)$$

for the moment estimator. We assume that  $\epsilon$  is chosen small enough for the inverse in Eq. (3.9) to exist. A precise condition can be derived by rewriting the convolution in this equation in the form (cf. Section 3 of Part I)

$$(\kappa * \rho^{(m)})(\mathbf{r}) = \int_0^{2\pi} \int_0^\omega d\theta \left( C_f \sin \theta + C_b \tan \theta \right) \int_0^z dz' \rho^{(m)}(\hat{\mathbf{r}}(\mathbf{r}; \theta, \phi, z')), \quad (3.10)$$

which yields

$$\left| (\kappa * \rho^{(m)})(\mathbf{r}) \right| \leq 2d_z \rho_{\max}$$

where  $d_z$  is the depth of the sample and  $\rho_{\max}$  the maximum value of the density  $\rho$ . So the inverse above exists if  $\epsilon \leq (2d_z \rho_{\max})^{-1}$ .

If in the expressions Eq. (3.8)–(3.9) only first order terms in  $\epsilon$  are taken into account and  $\rho^{(c)}$  or  $\rho^{(m)}$  is replaced by  $f$  in the RHS of these equations, respectively, we recover the approximation Eq. (2.6). It is therefore to be expected that the moment and cumulant estimators may give accurate results for a larger range of values of  $\epsilon$  than the estimator used in Part I. This will be investigated further in Section 5.

## 4. Computation by iterative algorithms

After discretization of equations Eq. (3.8)–(3.9), a finite system of nonlinear equations of the form

$$R_{ijk} = F_{ijk} G\left((K * R)_{ijk}\right), \quad (i, j, k) \in \mathbb{I} \quad (4.1)$$

results, where  $G(x) = \exp(\epsilon x)$  and  $G(x) = (1 - \epsilon x)^{-1}$ , respectively, with  $K * R$  the discrete convolution of the 3D arrays  $K$  and  $R$ . The following result is immediate.

**Lemma 4.1.** *The equations Eq. (4.1) have a unique solution.*

**Proof.** We consider successive values of the depth variable  $k$ . Starting at  $k = 1$ , we have

$$R_{ij1} = F_{ij1} G\left((K * R)_{ij1}\right).$$

Now, suppressing the summation limits in the  $i$  and  $j$  direction, we have

$$(K * R)_{ij1} = \sum_{i', j'} \sum_{k'=1}^{M_z} K_{i'j'k'} R_{i-i', j-j', 1-k'},$$

which equals zero because  $R_{ijk} = 0$  for  $k \leq 0$ . Since  $G(0) = 1$  for both estimators, we get

$$R_{ij1} = F_{ij1}. \quad (4.2)$$

Next, observe that for  $k \geq 2$ , we have

$$(K * R)_{ijk} = \sum_{i', j'} \sum_{k'=1}^{k-1} K_{i'j'k'} R_{i-i', j-j', k-k'}, \quad (4.3)$$

so that there are only nonzero contributions from the previous  $k - 1$  vertical layers to the convolution. This means that Eq. (4.1) can be solved successively for layer 1, 2, ...,  $N_z$ , e.g.

$$R_{ij2} = F_{ij2} G\left(\sum_{i', j'} K_{i'j'1} F_{i-i', j-j', 1}\right), \quad (4.4)$$

where we have used the previous result Eq. (4.2). The same argument shows that for any  $n$ ,  $R_{ijn}$  can be uniquely expressed in terms of the values in the previous  $n - 1$  layers of the signal array  $F$ . This completes the proof. ■

The equations Eq. (4.1) can be solved by Picard iteration [3], with  $F_{ijk}$  as the initial estimate:

$$\begin{aligned} R_{ijk}^{(1)} &= F_{ijk}, \\ R_{ijk}^{(n)} &= F_{ijk} G \left( (K * R^{(n-1)})_{ijk} \right), \quad n = 2, 3, \dots \end{aligned} \quad (4.5)$$

Each iteration step involves the computation of the discrete convolution  $K * R^{(n-1)}$  of the estimate  $R^{(n-1)}$  of the previous iteration (with the same convolution kernel  $K$ ) which can be efficiently computed by the FFT. The first iterate of Eq. (4.5) with  $G(x) = 1 + \epsilon x$  coincides with the discrete analogon of Eq. (2.6) and is the approximation used in Part I.

The question of convergence of the iteration Eq. (4.5) is answered by the following proposition.

**Proposition 4.2.** *The iterates  $R_{ijk}^{(n)}$  of Eq. (4.5) converge in a finite number of  $N_z$  steps towards the unique solution of Eq. (4.1). The convergence is monotonous, that is,  $R_{ijk}^{(n)} \geq R_{ijk}^{(n-1)}$ .*

**Proof.** We will prove the following assertion: after  $n$  iterations, the array elements  $R_{ijk}^{(n)}$  in the layers 1 to  $n$  have the correct values, that is, coincide with the solution of Eq. (4.1). We use induction on  $n$ . The main ingredient is again Eq. (4.3), which for  $k = 1$  has to be read as  $(K * R)_{ij1} = 0$ . The initial estimate

$$R_{ijk}^{(1)} = F_{ijk},$$

is correct for  $k = 1$ , see Eq. (4.2). Next assume that  $R_{ijk}^{(n-1)}$  is correct for  $k = 1, 2, \dots, n-1$ . Then, since  $(K * R^{(n-1)})_{ijk}$  involves only layers  $1, 2, \dots, k-1$  of the array  $R^{(n-1)}$ , we can write for  $k = 1, 2, \dots, n$ ,

$$R_{ijk}^{(n)} = F_{ijk} G \left( (K * R^{(n-1)})_{ijk} \right) = F_{ijk} G \left( (K * R)_{ijk} \right) = R_{ijk}.$$

So the induction hypothesis  $R_{ijk}^{(n-1)} = R_{ijk}$  for  $k = 1, 2, \dots, n-1$  yields  $R_{ijk}^{(n)} = R_{ijk}$  for  $k = 1, 2, \dots, n$ . This proves the assertion.

Finally, monotonicity of the iterates is easily proved by induction as well. First, using that  $G$  is increasing,

$$R_{ijk}^{(2)} = F_{ijk} G \left( (K * R^{(1)})_{ijk} \right) \geq F_{ijk} = R_{ijk}^{(1)}.$$

Next, assume that  $R_{ijk}^{(n)} \geq R_{ijk}^{(n-1)}$  (induction hypothesis). Then, using (i) nonnegativity of the convolution kernel (ii) the fact that  $G$  is increasing and (iii) the induction hypothesis, we deduce

$$R_{ijk}^{(n+1)} = F_{ijk} G \left( (K * R^{(n)})_{ijk} \right) \geq F_{ijk} G \left( (K * R^{(n-1)})_{ijk} \right) = R_{ijk}^{(n)},$$

and we are done. ■

In the next section we apply the iterative procedure of this proposition for improving the image restorations as described in Part I. We will see that only a few iterations are needed for obtaining accurate results. If this were not the case, and the full  $N_z$  iterations would be needed, then the complexity of our algorithm would increase from  $O(N_z \log N_z)$  (single convolution) to  $O(N_z^2 \log N_z)$ , and the advantage of our method over the layer method ‘with condensation’ of Visser et al. [6], which has complexity  $O(N_z^2)$ , would be lost.

A final result concerns the relative ordering of the two estimators considered.

**Proposition 4.3.** *The estimators  $\rho^{(m)}$  and  $\rho^{(c)}$  satisfy the inequality*

$$\rho^{(c)} \leq \rho^{(m)}.$$

This can be proved by complete induction just as in the proof of Proposition 4.2. It seems very hard to obtain any general statement as to the ordering of these estimators with respect to the *exact* solution  $\rho$ . In the case when the exact density  $\rho$  does only depend on  $z$  one may show by convexity arguments that

$$\rho^{(c)} \leq \rho \leq \rho^{(m)}$$

pointwise (that is, for every  $z$ ). In that case it is also clear that the cumulant estimator is more accurate than the approximation (2.6). For the examples with densities varying in the  $x, y$ -directions presented below these inequalities are found to be satisfied as well.

## 5. Restoration of a test image

In this section we consider a test density ('trig image')  $\rho(\mathbf{r})$  with a sinusoidal spatial variation, already used in Part I,

$$\rho(\mathbf{r}) = \frac{1}{4} \cos(2\pi n_x x/d_x) \cos(2\pi n_y y/d_y), \quad (5.1)$$

where  $d_x$  and  $d_y$  are the spatial dimensions of the sample in the  $x$ - and  $y$ -directions. Signal data  $F_{ijk}$  were generated by numerically computing the integrals in Eq. (2.1) for a number of equidistant 3D positions. The parameters were chosen as follows:  $d_x = d_y = 1.0$ ,  $d_z = 0.1$ ,  $N_x = N_y = 128$ ,  $N_z = 8$ ,  $\omega = 1.04719$ ,  $n_x = n_y = 8$ . We computed the relative root mean square error

$$\mathcal{E}(z) := \left( \frac{\sum_{x=1}^{N_x} \sum_{y=1}^{N_y} \{\rho(x, y, z) - \tilde{\rho}(x, y, z)\}^2}{\sum_{x=1}^{N_x} \sum_{y=1}^{N_y} \{\rho(x, y, z)\}^2} \right)^{\frac{1}{2}}, \quad (5.2)$$

between original density  $\rho$  and restored density  $\tilde{\rho}$  at each plane  $z = \text{constant}$ . Computations were performed on a SPARC workstation (35 Mhz, 26 MIPS), taking about one minute per iteration step (see Table 2 in Part I).

$\epsilon z$	signal error	iter = 1	iter = 2	iter = 3
0.0000	0.000	0.000	0.000	0.000
0.0625	0.116	0.004	0.004	0.004
0.1250	0.218	0.006	0.016	0.016
0.1875	0.305	0.025	0.041	0.045
0.2500	0.382	0.065	0.065	0.090
0.3125	0.450	0.127	0.075	0.153
0.3750	0.509	0.200	0.056	0.236
0.4375	0.560	0.278	0.026	0.330

**Table 1.** *Signal error and restoration errors by the moment estimator  $\rho^{(m)}$  after one, two and three iterations as a function of the effective depth  $\epsilon z$ .*

$\epsilon z$	signal error	iter = 1	iter = 2	iter = 3
0.0000	0.000	0.000	0.000	0.000
0.0625	0.116	0.010	0.010	0.010
0.1250	0.218	0.035	0.022	0.022
0.1875	0.305	0.080	0.047	0.046
0.2500	0.382	0.141	0.089	0.084
0.3125	0.450	0.213	0.146	0.136
0.3750	0.509	0.286	0.213	0.198
0.4375	0.560	0.357	0.283	0.265

Table 2. Signal error and restoration errors by the cumulant estimator  $\rho^{(c)}$  after one, two and three iterations as a function of the effective depth  $\epsilon z$ .

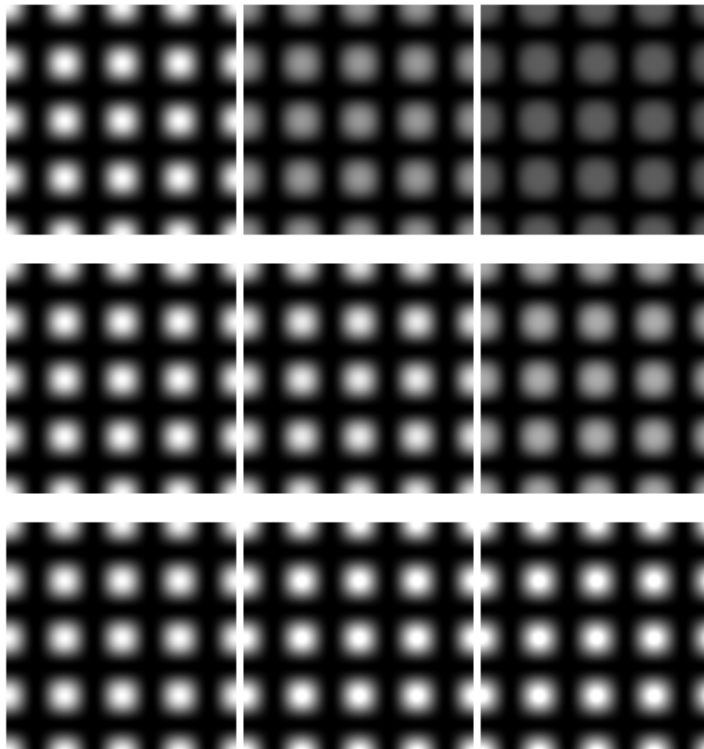


Figure 2. Restoration of the trig image.

First row: the attenuated test images; second row: restoration by the cumulant estimator ( $iter = 2$ ); third row: restoration by the moment estimator ( $iter = 2$ ). In each row, the first, fourth and seventh layer is displayed from left to right. The original image in each layer is identical to the first image in row 1.

Results are shown in Table 1 for the moment estimator Eq. (3.9) and in Table 2 for the cumulant estimator Eq. (3.9). In the case of the moment estimator the errors first decrease and then start to grow again after the third iteration. This is due to the fact that the initial estimate  $f(\mathbf{r})$  is smaller than the exact density  $\rho(\mathbf{r})$  (this is obvious from Eq. (2.1)–(2.3)),

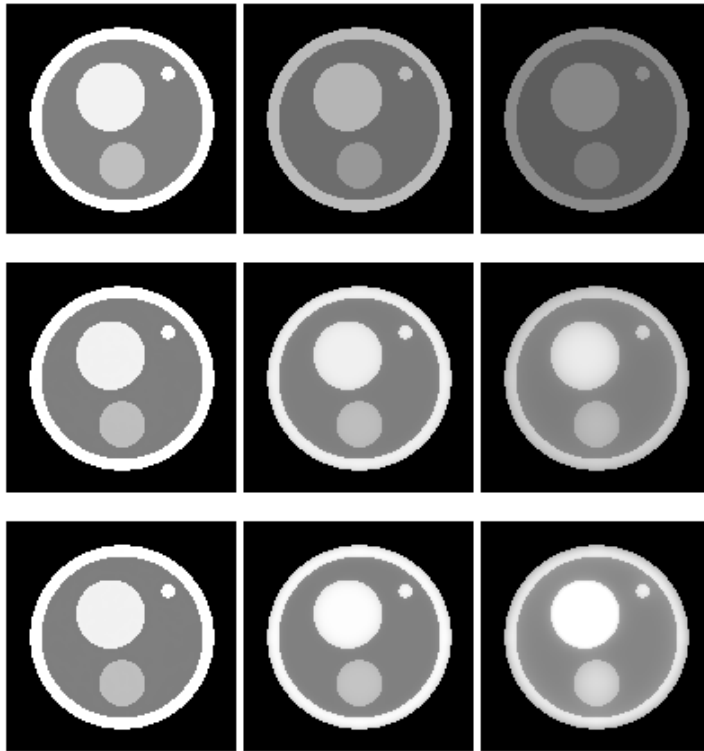


Figure 3. Restoration of the circle image.

First row: the attenuated test images; second row: restoration by the cumulant estimator ( $iter = 2$ ); third row: restoration by the moment estimator ( $iter = 2$ ). In each row, the first, fourth and seventh layer is displayed from left to right. The original image in each layer is identical to the first image in row 1.

so that at first the iterates underestimate the true solution. Because of the monotonicity property the iterates always increase so that (if the solution  $\rho^{(m)}$  is larger than the true  $\rho$ , which is apparently the case here) they will start to overestimate the true density. The cumulant estimator  $\rho^{(c)}$  underestimates the true density, and the values were stable within an accuracy of three digits after the third iteration. For comparison we give in column 2 of the Tables the error *before* restoration, denoted by ‘signal error’ and computed according to (5.2) with  $\tilde{\rho}$  replaced by  $f$ .

Comparing the numbers in Table 4 of Part I, we conclude that both the moment estimator with  $iter = 1, 2$  and cumulant estimator with  $iter \geq 2$  are more accurate than the layer method of [6] which gives a restoration error of 0.301 at the deepest layer. From the Tables it is clear that the moment estimator, when run to convergence, overestimates the exact image densities. The first iterate, however, underestimates the exact values. Therefore, in case of the moment estimator, we take the reconstruction corresponding to the intermediate value  $iter = 2$ , which gives the best results.

In Figure 2 we show the corresponding restored images. We rescale the restored values of the densities to make sure that they occupy the complete grey-scale, which consists of the set of integer values from 0 to 255. In order to avoid that a few outliers cause a large

visual degradation of the resulting images, we constrained the approximate solutions  $\tilde{\rho}$  to lie between the known lower and upper bounds, i.e.  $0 \leq \tilde{\rho} \leq 1$ . In each row, the first, fourth and seventh layer is displayed from left to right, out of a total of 8 depth layers. Since the exact density  $\rho(\mathbf{r})$  does not depend on  $z$ , the original image in each layer is identical to the first image in row 1. The first row contains the attenuated test images  $f(\mathbf{r})$ , the second row the restoration by the cumulant estimator and the third row the restoration by the moment estimator, both after two iterations. The images which are restored by the cumulant estimator are virtually identical to those of the layer method of Visser et al. [6], cf. Figure 4 of Part I. Clearly the largest improvement in restoration quality has been obtained by using the moment estimator. The reconstruction is not perfect, however: the central regions in the centers of the light circular regions are slightly overestimated. The calculations made here for the trig image have been repeated for the ‘circle image’ used in Part I, leading to similar conclusions: the reconstruction errors are smallest when using the moment estimator with  $iter = 2$ , but the reconstructed images still show some differences when compared to the original images, see Figure 3. Nevertheless, a considerable improvement in restoration accuracy has been obtained by using the estimators developed here, which in addition are efficiently computable by using FFT methods.

## 6. Summary

In this paper we describe a refinement of the method developed in Part I for attenuation correction in Fluorescence Confocal Microscopy using Fast Fourier Transform methods. Our approach, valid for weak attenuation, consists in multiplying the measured fluorescent intensity by a correction factor involving a convolution integral of the measured signal, which can be computed efficiently by an FFT-based algorithm. By a statistical reformulation of the problem we derive first order moment and cumulant estimators leading to a nonlinear integral equation for the unknown fluorescent density, which is solved by an iterative method. The algorithm is as follows:

- Read the measured data  $F_{ijk}, i = 1, \dots, N_x, j = 1, \dots, N_y, k = 1, \dots, N_z$ .
- Iteratively compute

$$R_{ijk}^{(n)} = F_{ijk} G \left( (K * R^{(n-1)})_{ijk} \right), \quad n = 2, 3, \dots$$

where  $R_{ijk}^{(1)} = F_{ijk}$ , and  $G(x) = (1 - \epsilon x)^{-1}$  or  $G(x) = \exp(\epsilon x)$  for the moment and cumulant estimator, respectively.

In each iteration the convolution of the previous estimate is computed by means of the FFT (using the same kernel  $K$  of Eq. (2.11)). The first iterate of the new estimators coincides with the approximation used in Part I for very weak attenuation. It turns out that the moment estimator with two iterations gives the best results, which are more accurate than the layer method of [6]. Since only two iterations are needed, the advantage in computational efficiency over the layer method is retained. We conclude therefore that the combined results of Part I and this paper provide an efficient and accurate method for attenuation correction in confocal microscopy.

## References

1. Brakenhoff G.J., P. Blom and P. Barends (1979). Confocal scanning light microscopy with high aperture immersion lenses. *J. of Microscopy* 117, pp. 219-232.
2. Lukacs E. (1960). *Characteristic Functions*. Griffin, London.

3. Ortega J.M. and W.C. Rheinboldt (1970). *Iterative Solution of Nonlinear Equations in Several Variables*. Ac. Press, New York.
4. Press W.H., B.P. Flannery, S.A. Teukolsky and W.T. Vetterling (1986). *Numerical Recipes, the Art of Scientific Computing*. Cambr. Univ. Press, New York.
5. Roerdink J.B.T.M. and M. Bakker. An FFT-based method for attenuation correction in fluorescence confocal microscopy. *J. Microscopy* 169, 1993, pp. 3-14.
6. Visser T.D., F.C.A. Groen and G.J. Brakenhoff (1991). Absorption and scattering correction in fluorescence confocal microscopy. *J. Microscopy* 163, pp. 189-200.
7. Wilson T. and C.J.R. Sheppard (1984). *Theory and Practice of Scanning Optical Microscopy*. Acad. Press, New York.